Why models perform differently on particulate matter over East Asia? – A multi-model intercomparison study for MICS-Asia III

Jiani Tan[1], Joshua S. Fu[1], Gregory R. Carmichael[2], Syuichi Itahashi[3], Zhining Tao[4], Kan Huang[1,5], Xinyi Dong[1], Kazuyo Yamaji[6], Tatsuya Nagashima[7], Xuemei Wang[8], Yiming Liu[8], Hyo-Jung Lee[9], Chuan-Yao Lin[10], Baozhu Ge[11], Mizuo Kajino[12], Jia Zhu[11], Meigen Zhang[11], Hong Liao[13] and Zifa Wang[11]

[1] Department of Civil and Environmental Engineering, University of Tennessee, Knoxville, TN, 37996, USA
[2] Center for Global and Regional Environmental Research, University of Iowa, Iowa City, IA, 52242, USA
[3] Central Research Institute of Electric Power Industry, Abiko, Chiba, 270-1194, Japan
[4] Universities Space Research Association, Columbia, MD, 21046, USA
[5] Department of Environmental Science and Engineering, Fudan University, Shanghai, 200433, China
[6] Graduate School of Maritime Sciences, Kobe University, Kobe, Hyogo, 658-0022, Japan
[7] National Institute for Environmental Studies, Tsukuba, Ibaraki, 305-8506, Japan
[8] Institute for Environment and Climate Research, Jinan University, Guangzhou, 511443, China
[9] Department of Atmospheric Sciences, Pusan National University, Busan, 609-735, South Korea
[10] Research Center for Environmental Changes Academia Sinica, 11529, Taiwan
[11] Institute of Atmospheric Physics, Chinese Academy of Science, 100029, China
[12] Meteorological Research Institute, Japan Meteorological Agency, 305-0052, Japan
[13] School of Environmental, Science and Engineering, Nanjing University of Information Science & Technology, Nanjing, 210044, China

Correspondence to: Joshua S. Fu (jsfu@utk.edu)

Abstract. This study compares the performances of twelve regional chemical transport models (CTM) from the third phase of Model Inter-Comparison Study for Asia (MICS-Asia III) on simulating the particulate matter (PM) over East Asia (EA) in 2010. The participating models include WRF-CMAQ (v4.7.1 and v5.0.2), WRF-Chem (v3.6.1 and v3.7.1), GEOS-Chem, NHM-Chem, NAQPMS and NU-WRF. This study investigates three model processes as the possible reasons for different model performances on PM: (1) Models perform very differently in the gas-particle conversion of sulphur (S) and oxidized nitrogen (N). The model differences in sulphur oxidation ratio (50%) are of the same magnitude as that in SO_4^{2-} concentrations. The gas-particle conversion is one of the main reasons for different model performances on fine mode PM. (2) Models without dust emissions/modules can perform well on PM_{10} at non-dust-affected sites but largely underestimate (upmost 50%) the PM_{10} concentrations at dust sites. The implementation of dust emissions/modules in models has largely improved the model accuracies at dust sites (reduce model bias to -20%). However, both the magnitudes and distributions of dust pollution are not fully captured. (3) The amounts of modelled depositions vary among models by 75%, 39%, 21%

and 38% for S wet, S dry, N wet and N dry depositions, respectively. Large inter-model differences are found in the washout ratios of wet deposition (at most 170% in India) and dry deposition velocities (general 0.3-2 cm s^{-1} differences over inland regions).

1 Introduction

Atmospheric pollution due to particulate matter (PM) has raised world-wide attention for its relationship with environmental and public health issues (Fuzzi et al., 2015;Nel, 2005). Fine particles ($PM_{2.5}$) are associated with cardiovascular and respiratory related cancer and premature deaths (Hoek and Raaschou-Nielsen, 2014;Knol et al., 2009). Outdoor $PM_{2.5}$ pollution is estimated to cause 2.1-5.2 million premature deaths worldwide annually (Lelieveld et al., 2015;Rao et al., 2012;Silva et al., 2013). It accounts for eight percent of global mortality in 2015 and ranks fifth in the global mortality risk (Cohen et al., 2017). East Asia (EA) has been suffering from severe PM pollution due to anthropogenic emissions and natural dust emissions (Akimoto, 2003). China and India are the top two countries suffering from outdoor air pollution, which altogether account for 20% of global mortalities caused by $PM_{2.5}$ exposure in 2010 (Lelieveld et al., 2015). The mixing of dust with anthropogenic pollutants can even enlarge the effects of pollution (Li et al., 2012). However, the impact evaluation of PM pollution is of high uncertainty due to unclearness in the toxicity of PM components (Lippmann, 2014) and difficulty in the measurement and prediction of PM concentrations.

For a better understanding of PM pollution, modelling approach has been adopted to study the spatial distributions of PM with the aid of measurements. Multi-model ensemble approach, which interprets modelling results with combined information from several models, has been proven to increase the reliability of model accuracy (Tebaldi and Knutti, 2007). This method has been widely used for studies in Europe (Bessagnet et al., 2016;Vivanco et al., 2017) and at global scales (Lamarque et al., 2013;Galmarini et al., 2017) on air quality issues. The Model Inter-Comparison Study Asia Phase (MICS-Asia) aims at understanding the air quality issues over EA. The first phase of MICS-Asia (MICS-Asia I) was carried out in the 1990s with eight regional chemical transport models (CTMs). The study focused on air pollution issues related to sulphur (S) (including SO_2, SO_4^{2-} and wet SO_4^{2-} deposition). The second phase of MICS-Asia (MICS-Asia II) was launched in early 2000s with nine CTMs (Carmichael and Ueda, 2008). The study covered the chemistry and transport of S, nitrogen (N), PM and acid deposition. Multi-model results on

SO_4^{2-}, NO_3^- and NH_4^+ (SNA) were evaluated with measurements from fourteen sites of Acid Deposition Monitoring Network in East Asia (EANET) and the Fukue site in Japan. However, a non-exhaustive evaluation on PM_{10} concentrations in China with scarce datasets left an unclear view of models' ability in this area, a region recognized as one of the most heavily polluted in EA. Meanwhile, model results were found with high inconsistencies on simulating both gas and aerosol phases of S and N (Hayami et al., 2008). Further efforts are needed to investigate the reasons for model differences to improve model accuracies.

This study compares the performances of twelve regional models participated in the third phase of MICS-Asia (MICS-Asia III) on simulating PM over EA. The comparison among models aims at identifying the reasons for different model performances. The models involved in this study include Weather Research and Forecasting Model (WRF) coupled with Community Multiscale Air Quality Modeling (CMAQ) (version 4.7.1 and v5.0.2), WRF model coupled with Chemistry (WRF-Chem) (v3.6.1 and v3.7.1), Goddard Earth Observing System coupled with Chemistry (GEOS-Chem), Non-Hydrostatic Model coupled with Chemistry (NHM-Chem), Nested Air Quality Prediction Modeling System (NAQPMS) and NASA-Unified WRF (NU-WRF). The model performance on simulating PM has been reported in a companion paper (Chen et al., 2019). The main findings are described in sect. 3.1. Sections 3.2-3.4 examine the influences of three model processes on model performances: (1) Formation of fine particles (PMF): model differences in the gas-particle conversion. (2) Formation of coarse particles (PMC): model improvements by implementing dust emissions/modules on simulating PM and the remaining problems. (3) Removal processes of particles from the atmosphere: uncertainties lay on the efficiencies of wet and dry depositions. Section 4 concludes the findings of this study and provides suggestion for further study.

2 Methodology

2.1 Framework of MICS-Asia

MICS-Asia is a model intercomparison study with contributions from international modelling groups to simulate the air quality and deposition over EA. MICS-Asia I focused on air quality issues related to S. The multi-model performances on simulating SO_2 and SO_4^{2-} concentrations and SO_4^{2-} wet deposition were evaluated with observation from eighteen stations (Carmichael et al., 2002). A source-receptor relationship of S deposition was developed based on the sensitivity

97 simulations for seven prescribed receptor regions: Komae, Oki, Fukue, Yangyang, Beijing,
98 Nanjing and Taichung (Carmichael et al., 2002).

99 MICS-Asia II was initiated in 2003. Nine regional models simulated the air qualities for
100 four months (March, July and December of 2001 and March of 2002) to study the chemistry and
101 transport of air pollutants and acid deposition (Carmichael and Ueda, 2008). All modelling groups
102 were enforced to use the same emission: the Transport and chemical Evolution over the Pacific
103 (TRACE-P) emission of 2000, and common IC/BC to facilitate a comparison on the physical and
104 chemical mechanisms of models. The modelling species expanded to S, N, O_3, PM and acid
105 deposition. Model evaluations and major findings can be found in literature (Carmichael et al.,
106 2008;Fu et al., 2008;Han et al., 2008;Hayami et al., 2008).

107 MICS-Asia III is launched in 2010. The simulation time covers the whole year of 2010.
108 All modelling groups are required to use the prescribed anthropogenic emissions and natural inputs
109 (including biogenic emissions, biomass burning emissions and volcanic SO_2 emissions. Dust and
110 sea-salt emissions are produced by the corresponding modules in different models) (Li et al., 2017).
111 Three purposes are set for this project– topic I: evaluating the strengths and weaknesses of current
112 multi-scale air quality models in simulating air qualities over EA and providing suggestion to
113 reduce uncertainty for future simulations, topic II: developing a reliable anthropogenic emission
114 inventory for EA, topic III: investigating the interaction of aerosol-weather-climate by using online
115 coupled air quality models. This study focuses on topic I.

116

117 **2.2 Model configurations**

118 The model set-up can be found in Table 1 of Chen et al. (2019). Fourteen modeling groups (M1-
119 M14) participated, but M3 and M9 are not included in this study due to uncompleted model
120 submission. M14 model has a smaller simulation domain than the others, therefore it is not
121 included in the multi-model mean (MMM) results. The gas and aerosol modules and dust schemes
122 employed by the participating models were introduced in detail in sect. 2.1 of Chen et al., 2019.
123 Following are the descriptions on the model set-up for wet and dry deposition.

124 Wet deposition removes gases and aerosols from the atmosphere by rain droplets, involving
125 both in-cloud scavenging (rainout) and below-cloud scavenging (washout). The gases in the

atmosphere are dissolved in the raindrop and then removed from the atmosphere. For the non-reactive gases, the removal rate depends on the solubility of gases and is a function of the Henry's Law. Particles take part in the cloud condensation nuclei in the presence of supersaturation water vapor and then grow into cloud droplets. In this study, only M2, M4, M6, M11 and M12 have submitted the main components of S and N depositions. All these models use the same wet deposition scheme based on Henry's law. The efficiency of wet deposition is assessed by the so-called "washout ratio", calculated as the ratio of particle concentrations in deposition to particle concentrations in surface air as shown in Eq. 1.

$$\lambda_{wet} = \frac{C_{depo}}{C_{surface\_air}} \times 100\% \quad (1)$$

where λ_{wet} (%) is the washout ratio for wet deposition, C_{depo} (μg m^{-3}) is the concentration of particles in deposition and $C_{surface\_air}$ (μg m^{-3}) is the concentration of particles at near surface atmosphere.

Dry deposition is mainly driven by turbulent and molecular diffusion processes. All models except M12 use the same dry deposition scheme from Wesely (1989). The dry deposition flux is proportional to the concentration of pollutants at height. The dry deposition velocity is calculated with Eq. 2.

$$V_d = -F_c / C_a \quad (2)$$

$$V_d = \frac{1.0}{r_{surf}+r_a+r_{bc}} \quad (3)$$

where F_c (mg m^{-2} yr^{-1}) is the dry deposition flux, V_d (cm s^{-1}) is the deposition velocity and C_a (μg m^{-3}) is the concentration of species at height. The negative mark indicates the direction of the dry deposition velocity. The V_d is determined by the resistance of air layer (r). The total r is composed of three factors (Eq. 3): the aerodynamic resistance (r_a), boundary layer resistance (r_{bc}) and canopy resistance (r_{surf}).

M12 uses the general approach from Wesely (1989) and updates by Zhang et al. (2003). Zhang et al. (2003) updates the value of non-stomatal resistance (R_{ns}), which is a component of R_{surf} related to the soil uptake and cuticle uptake of dry deposition. Model evaluation shows the updates can improve the model prediction on dry deposition velocities of SO_2 (Zhang et al., 2003).

2.3 Observation data

To make the discussion clear, we define the regions used in the following analysis here: northern EA (Russia and Mongolia), central EA (China), eastern EA (Japan and Korea) and southern EA (Cambodia, Lao PDR, Myanmar, Thailand, Vietnam, Indonesia, Malaysia and Philippines). Following monitoring datasets are used in the analysis in sects. 3.2-3.4: Air Pollution Indices (APIs) provides monthly average PM_{10} data from eighty-six sites (A1-A86 in Fig 1) (http://datacenter.mep.gov.cn/). This dataset has been widely used to study the PM pollution (Qu et al., 2010;Chen et al., 2008;Deng et al., 2011) as well as model evaluation (Wang et al., 2012;Xing et al., 2015) in China. It is replaced by the Air Quality Index (AQI) after 2013. The APIs data covers the eastern China well with intensively located sites, but sites in western China are very limited. EANET (E1-E54) provides monthly average concentrations of PM_{10}, SNA and S and N depositions from fifty-four sites (http://www.eanet.asia/, last access: 28 May 2018). For PM_{10}, this dataset has very limited number of sites in China. The sites are generally located along the east coast of China and couldn't well cover the areas with high PM_{10} pollution, such as the Hebei-Beijing-Tianjin (HBT) region (Fig. 1). And the data completeness in northern EA is not as satisfying as the other regions. Only three sites located in Rishiri (E15), Ochiishi (E16) and Oki (E21) in Japan have $PM_{2.5}$ observation during our study period. R1-R35 (green) are thirty-five Reference (Ref) sites provided by the Institute of Atmospheric Physics Chinese Academy of Science (IAP_CAS). The sites are concentrated in three regions: HBT region, Pearl River Delta (PRD) and Taiwan.

3 Result and discussion

3.1 Brief results of model performance evaluation

All models have submitted the monthly average concentrations of PM_{10}, $PM_{2.5}$ and SNA at surface layer except PM_{10} from M13 and NO_3^- and NH_4^+ from M10. Evaluation of model performance on aerosols can be found in our companion paper (Chen et al., 2019). Following are the main findings: the differences between MMM and observation/satellite data for the surface concentrations of PM_{10}, $PM_{2.5}$, SO_4^{2-}, NO_3^- and NH_4^+, and column integrated aerosol optical depth (AOD) were -32.6%, 4.4%, -19.1%, 4.9%, 14.0% and 18.7%, respectively (calculated with normalized mean

biases (NMBs)). PM_{10} concentrations were generally underestimated over the simulation domain. $PM_{2.5}$ concentrations were also underestimated over Eastern EA, but were well simulated in Central EA. Models failed to reproduce the high peaks of SO_4^{2-} concentration in Central EA, probably due to missing SO_4^{2-} formation mechanisms (such as heterogeneous SO_4^{2-} chemistry), which has been reported as an important formation pathway of SO_4^{2-} in China. NO_3^- concentrations were overpredicted by most models over the simulation domain and were associated with the underestimation of SO_4^{2-}. M7 and M8 models produced significantly lower NO_3^- concentrations than observations and other models, due to underestimation in NH_3 concentrations (might be caused by low NH_3 emission) and missing the N_2O_5 heterogeneous reaction that sever as an important formation pathway of NO_3^- (Chen et al., 2019). The spatial distributions of AOD were generally well simulated, but several models were found to underestimate the AOD values around the Himalaya mountains, Taklamakan Desert and Gobi Desert.

This study compares the model performances with global-scale model study. The Task Force on Hemispheric Transport of Air Pollution (TF HTAP) is an inter-comparison study of global and regional models to assess the impact of hemispheric transport of air pollutants on regional atmosphere. The second phase of HTAP (HTAP-II) involved more than twenty global models to simulate the air quality in 2010 (Galmarini et al., 2017). Most models utilize coarse-resolution grids at about 2°-3°. The HTAP-II and MICS-Asia III share some common points like using the same emission inventory in East Asia (Li et al., 2017) and using the same observation dataset to evaluate PM_{10} (more than 100 EANET and API sites) and $PM_{2.5}$ (two EANET sites) (Dong et al., 2018). The mean bias (MB) of PM_{10} over EA is -30.7 μg m^{-3} and -18.6 μg m^{-3} for HTAP-II and this study, respectively (values for sites used by both studies). And the MB of $PM_{2.5}$ is -1.6 μg m^{-3} and -4.3 μg m^{-3} for HTAP-II and this study, respectively. Both studies find underestimation of PM_{10} concentrations, while $PM_{2.5}$ concentrations are well produced. Models of MICS-Asia III perform slightly better than those of HTAP-II with lower model bias in PM_{10}, probably taking the advantage of finer resolutions of model grids.

The so-called "diagnostic evaluation" approach is adopted to check the model bias oriented by individual processes (Dennis et al., 2010). Although all modelling group are required to use the prescribed emission inventory, a mismatch was found during the temporal and vertical treatments of emission files by different modelling groups and has caused differences in the model inputs

(Itahashi et al., 2019). To avoid the possible impacts on inter-model comparison, we compare the indicators (i.e. sulphur oxidation ratio (SOR)) instead of direct model outputs (i.e. SO_4^{2-} concentrations) to focus on the differences caused by model mechanisms. The following three processes are examined:

(1) Formation of PMF: sect. 3.2 investigates the differences in the gas-particle conversion of S and N among different models.
(2) Formation of PMC: sect. 3.3 assesses the model abilities in reproducing the spatial and temporal distributions of PM in regions affected by dust storm. A comparison is conducted between models with and without dust emissions/modules.
(3) Removal of particles from the atmosphere: sect. 3.4 compares the model performances in simulating the amounts of deposition and the efficiencies of wet and dry depositions.

3.2 Gas-particle conversion

The following two indicators are calculated to illustrate the gas-particle conversions of S and N.

$$SOR = \frac{n\text{-}SO_4{}^{2-}}{n\text{-}SO_4{}^{2-} + n\text{-}SO_2} \quad (4)$$

$$C(NO_2) = \frac{n\text{-}NO_3{}^{-}}{n\text{-}NO_3{}^{-} + n\text{-}NO_2} \quad (5)$$

where $n\text{-}SO_4^{2-}$, $n\text{-}SO_2$, $n\text{-}NO_3^{-}$ and $n\text{-}NO_2$ (mole m^{-3}) are the mole concentrations of SO_4^{2-} particle, SO_2 gas, NO_3^{-} particle and NO_2 gas. The $C(NO_2)$ (%) indicator only has NO_3^{-} and NO_2 in the denominator due to the limitation of observation data. But it still can portrait the conversion of N between gas phase and particle phase.

Figures 2 and 3 show the distributions of *SOR* and $C(NO_2)$ values of models. The *SOR* values are lowest around the HBT region in north-eastern China (10-40%) and highest in south-western China (60-80%) (Fig. 2). The X-CMAQ models (including WRF-CMAQ and RAMS-CMAQ) produce similar *SOR* patterns, except that the CMAQv5.0.2 models (M1 and M2) predict 10% higher *SOR* in the HBT region than the CMAQv4.7.1 models (M4, M5 and M6). CMAQv502 updated the production of SO_4^{2-} in the aqueous reaction of the older version (Appel et al., 2013; Fountoukis and Nenes, 2007). The explicit treatment of Fe and Mn allows more consistent

240 treatment of aqueous reaction from SO_2 to SO_4^{2-}. For the X-Chem models (including WRF-Chem,
241 GEOS-Chem and NHM-Chem), the two WRF-Chem models (M7 and M8) produce similar
242 magnitudes and distributions of *SOR* in all regions, except the south-western China (around Tibet
243 in Fig. 1) and the open oceans, while the NHM-Chem (M12) and GEOS-Chem (M13) models
244 produce slightly higher *SOR* values over the whole simulation domain. The differences between
245 the X-CMAQ and the X-Chem models are significant over the inland regions of northern and
246 eastern China, Japan and southern EA. The X-CMAQ models generally predict 5-20% higher *SOR*
247 values than the X-Chem models. Similarly, the X-CMAQ models generally give 20% higher
248 $C(NO_2)$ values than the WRF-Chem models, especially in eastern EA (Fig. 3). The $C(NO_2)$ of M8
249 is extremely low due to unreasonably low NO_3^- concentrations.

250 Figure 4 shows the gas-particle conversions of S and N by models and observation at the
251 EANET sites. The red bars represent concentrations of gases and the black bars represent
252 concentrations of aerosols. The values with blue color above the bars are observed and modelled
253 *SOR* and $C(NO_2)$ values. Results for individual sites are available in supplementary Fig. S1.
254 According to Fig. 4(a), the total amount of S (SO_2 gas+SO_4^{2-} particle) is about 0.15 μmole(S) m^{-3}.
255 Most models have biases on this value, especially the moderate underestimation by M7, M8 and
256 M13. On the other hand, the *SOR* value (0.25) is well simulated by M1 (0.26), M2 (0.20), M10
257 (0.29) and M13 (0.26). Other models generally under-predict the *SOR* value except M12 (0.33)
258 and M14 (0.57). The WRF-CMAQv5.0.2 models (M1 and M2) produce higher *SOR* than WRF-
259 CMAQv4.7.1 models (M4, M5 and M6), probably attributed to the updates in the formation
260 pathway of SO_4^{2-}.

261 Figure 4(b-e) show the results in different regions. In northern EA, the total amount of S is
262 underestimated by all models except M13 and M14. However, the *SOR* value (0.12) is well
263 reproduced by most models (0.08-0.20) except M12 (0.25) and M10 (0.32). There is only one site
264 available for central EA. Most models (except M12 and M13) have largely underestimated the
265 *SOR* value, while M14 has largely overestimated it. For eastern EA, the total amount of S is well
266 captured by all models except M11, M12 and M14. The *SOR* value (0.55) is generally
267 underestimated by all models except M10 (0.55) and M14 (0.71). For southern EA, the total
268 amount of S is generally overestimated by all models except M13, while the *SOR* value is
269 underestimated by all models except M13 and M14. Overall, the models have both positive and

negative biases in simulating the total amounts of S, but generally underestimated the *SOR* values in all regions. Furthermore, the modelled *SOR* values vary largely among models (ranging from 0.12 to 0.57), resulting in a large inter-model difference (1sd% = 50%). This variation is of the same magnitude as the variation of SO_4^{2-} concentration (1sd% = 50% in supplementary Fig. S2). The results suggest that differences in gas-particle conversion among models could account largely for the models' inconsistency in simulating the SO_4^{2-} concentrations.

Figure 4(f-h) compares the gas-particle conversion of N with the $C(NO_2)$ indicator. Only one site in China and one site in Japan have both NO_2 and NO_3^- observations. At the Hongwen sites in China, all models except M5 underestimate the sum of NO_2 and NO_3^-, but the modelled $C(NO_2)$ values are close to the observation (0.18) except M5 (0.07), M8 (0.00) and M12 (0.40). Similar to the results of S conversion, the newer version of WRF-CMAQ model generally produces higher $C(NO_2)$ than the older version, but the differences between the two in $C(NO_2)$ are smaller than those in *SOR*. At the Banryu site in Japan, the sum of NO_2 and NO_3^- is well simulated by all models except M8. The $C(NO_2)$ (0.19) value is also well simulated by all models except M8 (0.00), M12 (0.53) and M14 (0.77). Overall, the model accuracy on $C(NO_2)$ is slightly higher than that on *SOR* according to the comparison with observed values. Models also have higher consistencies on $C(NO_2)$ than *SOR*. However, further validation is required due to the limited number of observations for the conversion of N.

Besides the inter-model differences in the pathways of SO_4^{2-} and NO_3^- formation, the interaction between aerosols and atmospheric oxidants can also affect the formation of aerosols (Liao et al., 2003). Aerosols affect the tropospheric oxidants (i.e. HO_x) budget by altering the photolysis rates and uptake of reactive gases (Tie et al., 2003; Li et al., 2018). In turn, the abundance of HO_x affects the gas-aerosol conversion of S and N. In addition, the conversion between sulfuric acid and SO_4^{2-} depends on the abundance of neutralizers such as Na^+ and NH_4^+

3.3 Implementation of dust emissions/modules in models

The PMC concentrations at surface layer are calculated by subtracting $PM_{2.5}$ from PM_{10}. Figure 5 shows the spatial distribution of annual average PMC of models. Most models show very low (< 2μg m^{-3}) concentrations of PMC around the Takalmakan Desert and the Gobi Desert in northern

China except M10, M11 and M14. These three models use dust emissions/modules in simulations (Chen et al., 2019). M12 also includes dust emissions, but its PM_{10} concentrations over northern China are much lower than the three models. The predicted PMC concentrations of the three models differ largely. The domain-average concentrations of PMC are 21, 7 and 12 μg m^{-3} for M10, M11 and M14, respectively. The distributions of PMC also differ largely over north-west China, where the impacts of dust are most significant. The differences among the models mainly come from the different parameterizations such as source functions, dust-lifting mechanisms and size distributions of particles (Chen et al., 2019). Different PMC concentrations are also found over oceans, mainly attributed to the sea-salt emissions in this study. The sea-salt emissions are parameterized in the models with various formula (Chen et al., 2019). In this study, the WRF-Chem models (M7 and M8) turned off the sea-salt emissions, thus their PMC concentrations over the oceans and seas are not defined. The two WRF-CMAQ models use the in-line sea-salt emission module of Gong (2003) and updated by Kelly et al. (2010). They predict consistent distributions of PMC over oceans. M10 and M11 use the same module as the CMAQ models (Gong, 2003), but produce higher PMC on oceans. M12 adopts the method of breaking wave over seashore by Clarke et al. (2006) and produces the highest PMC over oceans among all models.

The implementation of dust emission is expected to improve the model performances, but how significant could the improvement be? And can models predict the PM concentrations reasonably at regions affected by dust with current dust emissions/modules? To answer these questions, all sites are grouped to dust and non-dust sites according to their locations. The sites located in regions that have been reported to receive severe impacts and rapid deposition of dust are marked as dust sites (Shao and Dong, 2006) (grey-color shaded areas in Fig. 1). Figure 6(a-b) and Table 1 compare the model performances at the dust and non-dust sites. For the non-dust sites (Fig. 6(b)), most models have well captured the magnitudes of PM_{10} at the "API non-coastal, non-dust" sites (MB = -8% and NMB = -8%). The sites marked as "API coastal" sites, which are located close to the coastal regions, are all slightly underestimated by about 25 μg m^{-3} (30%). Similarly, the PRD and Taiwan sites, which are also located near the coastal regions, are all underestimated by about 20 μg m^{-3} (37%). Bias in sea-salt emissions is the possible reason. Sea-salt emission is reported to contribute to 20-40% of SNA and PM_{10} over coastal regions (Liu et al., 2015). Including the sea-salt emission in model simulation can improve the model accuracy with 8-20%

increase in PM_{10}, SNA, Na^+ and Cl^- (Kelly et al., 2010;Im, 2013). The influence of sea-salt emission is not the focus of this study, but further study is strongly recommended.

For the dust sites (Fig. 6(a)), most models have generally underestimated the PM_{10} concentrations by 10-40 μg m^{-3} (15-50%). And the three models with dust module perform better than the others at the dust sites, especially site A2, A30, A68, A69, R5 and R18. However, they miss the high PM_{10} concentrations at sites like R1-R3 and R11, and overestimate the PM_{10} concentrations at sites such as A60 and A80. This indicates that the dust emissions/modules involved in this study can't fully capture the magnitudes and distributions of dust pollution over EA. In addition, the modelled PMC differ a lot with different dust emissions/modules (Fig. 5). M10 model produces very high PMC over the whole eastern China, while M11 model only predicts high PMC around the HBT region. Overall, the model performance on PM over dust regions can be improved largely by including dust emissions/modules. However, the concentrations and distributions are not yet well captured and large inconsistencies are found among different dust emissions/modules.

Figure 6(c-d) compares the modelled monthly trends of PM_{10} with observations at the dust and non-dust sites and Fig. 6(e) shows the correlations (R) values between models and observation. For the non-dust sites (Fig. 6(d)), the trends are well caught by most models. The R values are close to 0.70 for all models except M7 (0.62), M8 (0.58) and M14 (0.63). The WRF-Chem models (M7 and M8) simulate too low PM_{10} concentrations in winter. M14 model overestimates the PM_{10} concentrations during March to May. Most models have much lower R values at the dust sites than the non-dust sites (Fig. 6(e)), due to underestimation of the PM_{10} concentrations during winter. For instance, R values of M10 drop from 0.7 at the non-dust sites to 0.11 at the dust sites. Spring (March, April and May) has the largest model biases at the dust sites, which is coincident with the dust storm season in Asia (Arimoto et al., 2006). M10 and M14 models perform well in most months at both the dust and non-dust sites, taking the advantage of their dust emissions/modules. But their R values at the dust sites are very low. Future study is strongly suggested on a better understanding of the seasonal variations of dust pollution.

3.4 Wet and dry depositions

Figure 7 and Table 2 show the model performance on wet deposition. For wet SO_4^{2-} deposition, despite that the two sites with highest deposition (E2 and E3) in China are underestimated, the

other sites are generally well simulated by MMM with a low MB of -8%. The individual model bias varies from -22% to 41%. The CMAQ models (M2, M4 and M6) all underestimate the wet SO_4^{2-} deposition. There are large differences between CMAQv4.7.1 and CMAQv5.0.2 in JP, where the CMAQv4.7.1 models (M4 and M6) slightly overestimate the wet SO_4^{2-} deposition at E19 and E23, while the CMAQv5.0.2 model (M2) slightly underestimates the value at these sites. The M11 model produces considerably higher wet deposition of SO_4^{2-} and NO_3^- than the other models in East EA. The possible reasons are discussed later. The MMM underestimates the NO_3^- wet deposition by 29%, due to large under-prediction in southern EA. The southern EA has several sites with very high deposition, such as E29 site in MY and E35 and E36 sites in PH, but all models fail to catch those high peaks. The individual model bias varies from -59% to 30% among models. M2, M4, M6 and M12 perform similarly with high underestimation ranging from 39% to 59%. The M11 is the only model that succeeds to capture the high wet NO_3^- deposition at E2 and E3 in CH, but it overestimates most sites in CH, JP and KR. In case of wet NH_4^+ deposition, the MMM generally underestimates the amount at all sites with a bias of -40%, especially at E2-E4 in CH, E45 in TH and E35 and E36 in PH. The individual model bias varies from -10% to -37%. The M2, M4 and M6 models perform similarly, while M11 and M12 models predict higher depositions at all sites. Overall, large inter-model disagreements are found in eastern EA for wet deposition of SO_4^{2-} and NO_3^- and in southern EA for the wet NH_4^+ deposition. The observation of dry deposition is composed by observed concentration of air pollutants and simulated deposition velocity. Since the EANET network only provides the former one, complete evaluation of the dry deposition is not available in this study (complete dry deposition with velocity is available after 2013).

Table 3 lists the domain-total annual-accumulated amounts of S and N depositions by models. The total wet S deposition (D_{Swet}) includes wet depositions of SO_2, H_2SO_4 and SO_4^{2-}. The total dry S deposition (D_{Sdry}) includes dry deposition of SO_2, H_2SO_4 and SO_4^{2-}. The total wet N deposition (D_{Nwet}) includes wet depositions of NO_3^-, NH_4^+, HNO_3, NH_3. The total dry N depositions (D_{Nwet}) includes dry deposition of NO, NO_2, NO_3^-, NH_4^+, HNO_3 and NH_3. D_{Swet} values range from 10.5 to 31.3 Tg(S) yr^{-1} among models (1sd%=75%). The estimation by M11 model is two folds higher than the other four models. The inter-model difference is significant even among the same type of models with different versions. The CMAQv4.7.1 models (M4 and M6) produce 12.5 Tg(S) yr^{-1} (M4) and 13.8 Tg(S) yr^{-1} (M6) of D_{Swet}, while the prediction by CMAQv5.0.2 model (M2) is 25% lower. Despite the large discrepancies in the total amount, all five models

agree that over 95% of D_{Swet} is wet SO_4^{2-} deposition. The total amounts of D_{Sdry} range from 4.3 to 10.6 Tg(S) yr^{-1} among models (1sd% =39%). M11 predicts higher D_{Sdry} than other models and the CMAQv5.0.2 model (M2) predicts 45% lower D_{Sdry} than the two CMAQv4.7.1 models (M4 and M6). Similar to D_{Swet}, all models have high agreements on the proportions of the components. D_{Nwet} range from 12.2 to 20.0 Tg(N) yr^{-1} among models (1sd%=21%). The CMAQ models (M2, M4 and M6) simulate close results (12-15 Tg(N) yr^{-1}), while M11 (20.0 Tg(N) yr^{-1}) and M12 (16.5 Tg(N) yr^{-1}) simulate slightly higher amounts. As for the proportion of components, M2, M4, M6 and M12 models predict high proportions of wet NO_3^- and wet NH_4^+ depositions (particle phase), while M11 model produces higher percentages of wet HNO_3 and wet NH_3 depositions (gas phase). D_{Ndry} range from 3.9 to 14.1 Tg(N) yr^{-1} (1sd%=38%). M12 gives a considerably lower amount than the other models. Models are quite consistent on the proportions of components. The amount of wet deposition is determined by the $C_{surface\_air}$ and λ_{wet} (mentioned in sec. 2.2). And in this study, $C_{surface\_air}$ may be partial influenced by different model inputs, caused by mismatch occurred in vertical and temporal allocation of emission inputs and employment of different mechanisms to produce dust and sea-salt emissions. Thus, we used λ_{wet}, instead of direct model outputs of wet deposition, as an indicator to reveal the inter-model differences on wet deposition in the following analysis. For the same reason, we used V_d as an indicator for inter-model comparison on dry deposition.

Figure 8(a-e) show λ_{wet} of S deposition (λs_{wet}) by models. The CMAQ models (M2, M4 and M6) have similar patterns in λs_{wet} over the inland regions, while M12 model predicts 30-90% lower ratios in India. M11 model generally predicts about 20-70% lower λs_{wet} than the other four models except India, where the difference could reach upmost 170%. For λ_{wet} of N deposition (λ_{Nwet}) (Fig. 8(f-j)), the CMAQv4.7.1 models (M4 and M6) and M12 perform similarly, but the CMAQv5.0.2 model (M2) predicts 30% lower λ_{Nwet} in India, Japan and Korea. M11 generally predicts lower ratios in India (60% lower), Indonesia and Philippines (120% lower) than the CMAQ models. Figure 9 shows the spatial distributions of V_d. For V_d of S deposition (V_{Sd}) (Fig. 9(a-e)), the CMAQ models (M2, M4 and M6) simulate very similar spatial distributions. M11 and M12 models predict 0.5 cm s^{-1} lower V_{Sd} than the CMAQ models over the whole inland regions, especially in east China and India peninsular. For V_d of N deposition (V_{Nd}) (Fig. 9(f-j)), the CMAQ models (M2, M4 and M6) predict very similar distributions. M11 and M12 predict about 0.3 cm s^{-1} and 1-2 cm s^{-1} lower V_{Nd} than the CMAQ models over the inland regions. Both λ_{wet} and V_d of M11 are much lower than

the other models, especially over eastern EA. And this is a possible reason for the biased performance of M11 on wet deposition (Fig. 7). Overall, large inter-model differences are found in predicting both the amounts of depositions and the efficiencies of depositions.

4 Conclusion

The topic I of the MICS-Asia III aims at (i) evaluating the strengths and weaknesses of current multiscale air quality models in simulating concentration and deposition fields over East Asia and (ii) providing suggestions for future model developments. This study compares the performances of twelve regional models for the prediction of PM concentrations over EA. The participating models includes WRF-CMAQ (v4.7.1 and v5.0.2), WRF-Chem (v3.6.1 and v3.7.1), GEOS-Chem, NHM-Chem, NAQPMS and NU-WRF. Three processes/mechanisms are investigated to identify the causes of inter-model differences:

(1) For the formations of PMF, *SOR* and $C(NO_2)$ values are used to demonstrate the inter-model differences in gas-particle conversions. The *SOR* values are generally underestimated by most models at the EANET sites. A generally trend is found that the WRF-CMAQv5.0.2 models produce the highest *SOR* values among all models, followed by the WRF-CMAQv4.7.1 models (10% lower in HBT region), the WRF-Chem models and other models (5-20% lower over inland regions). The inter-model variation on *SOR* (1sd% =50%) is of the same magnitude as that on SO_4^{2-} concentration. Similar results are found in $C(NO_2)$, but models have higher agreements on $C(NO_2)$ than *SOR*. The different treatments of gas-particle conversions account largely for the different model performances on PMF.

(2) For the formations of PMC, the models without dust emissions/modules generate very low ($<2\mu g\ m^{-3}$) PMC concentrations. They can well capture the PM_{10} concentrations at non-dust-affected sites but underestimate the PM_{10} concentrations at sites affected by dust storms by upmost 50%. This underestimation is largely improved by implementing dust emissions/modules (bias reduced to around -20%). However, both the magnitudes and distributions of dust pollution are not fully captured. In addition, models employing different dust emissions/modules show large disagreements on the distributions of PMC.

(3) For the removal of PM from the atmosphere, the amounts of atmospheric deposition vary largely among models (1sd%) by 75%, 39%, 21% and 38% for D_{Swet}, D_{Sdry}, D_{Nwet} and D_{Ndry},

respectively. The λ_{wet} and V_d indicators are used to exclude the influences brought by model inputs. For λ_{wet}, models agree more on the D_{Swet} than D_{Nwet}. The largest model inconsistencies are found in India (upmost 170%), Indonesia and Philippines (upmost 120%). For V_d, models differ more on D_{Ndry} than D_{Sdry}, which is opposite to λ_{wet}. The inter-model differences are widely found over the inland regions for D_{Sdry} (about 0.5 cm s^{-1}) and D_{Ndry} (0.3-2 cm s^{-1}).

The main contributions of this study are: (1) comparing the conversions of S and N between gas and particle phases among different models as well as with observations. The comparison with observation makes it possible to both quantify the inter-model differences and tell which module might be more reasonable; (2) Several new updates on dust modules have been published in recent literature, but there is limited study on the inter-comparison. This study provides an opportunity to bring together the new updates on dust modules/emission and review their performance in EA; (3) providing a comprehensive view on the total budget of S and N aerosols, by including the analysis on the removal processes. It turns out that this process brings significant uncertainties to inter-model differences. It should be noted that other factors such as vertical diffusion can also contribute to model differences. Meanwhile, this study focuses on comparing the model abilities in simulating PM in 2010. The chemical regimes may have changed drastically due the rapid changes of emissions and implementation of control policies in Asia. Studies on more recent years and heavily polluted episodes are under preparation.

Author Contributions. JT and JSf designed the study. JT processed and analysed the data. JSF, GRC, SI and ZT contributed to the results and discussions. JSF, ZT, KH, SI, KY, TN, YM, XW, YL, HJL, JEK, CYL, BG, MK, JZ, MZ, LH and ZW provided modelling data. All co-authors provided comments to the manuscript.

Data Availability. The observation data are introduced with details in supplementary sect. S2.1 with web links of public available datasets. The model data are available upon request.

Competing interests. The authors declare that they have no conflict of interest.

Acknowledgements. We thank all participating modeling groups of MICS-Asia III. We acknowledge the support by the Advanced Computing Facility (ACF), Joint Institute for Computational Sciences of the University of Tennessee. We also thank the support by the Oak Ridge National Laboratory for computational resources, which is supported by the Office of Science of the U.S. Department of Energy (contract DE-AC05-00OR22725).

Reference

Akimoto, H.: Global air quality and pollution, Science, 302, 1716-1719, DOI: 10.1126/science.1092666, 2003.

Appel, K. W., Pouliot, G. A., Simon, H., Sarwar, G., Pye, H. O. T., Napelenok, S. L., Akhtar, F., and Roselle, S. J.: Evaluation of dust and trace metal estimates from the Community Multiscale Air Quality (CMAQ) model version 5.0, Geoscientific Model Development, 6, 883-899, 10.5194/gmd-6-883-2013, 2013.

Arimoto, R., Kim, Y. J., Kim, Y. P., Quinn, P. K., Bates, T. S., Anderson, T. L., Gong, S., Uno, I., Chin, M., Huebert, B. J., Clarke, A. D., Shinozuka, Y., Weber, R. J., Anderson, J. R., Guazzotti, S. A., Sullivan, R. C., Sodeman, D. A., Prather, K. A., and Sokolik, I. N.: Characterization of Asian Dust during ACE-Asia, Global Planet Change, 52, 23-56, https://doi.org/10.1016/j.gloplacha.2006.02.013, 2006.

Bessagnet, B., Pirovano, G., Mircea, M., Cuvelier, C., Aulinger, A., Calori, G., Ciarelli, G., Manders, A., Stern, R., Tsyro, S., Vivanco, M. G., Thunis, P., Pay, M. T., Colette, A., Couvidat, F., Meleux, F., Rouil, L., Ung, A., Aksoyoglu, S., Baldasano, J. M., Bieser, J., Briganti, G., Cappelletti, A., D'Isidoro, M., Finardi, S., Kranenburg, R., Silibello, C., Carnevale, C., Aas, W., Dupont, J. C., Fagerli, H., Gonzalez, L., Menut, L., Prevot, A. S. H., Roberts, P., and White, L.: Presentation of the EURODELTA III intercomparison exercise - evaluation of the chemistry transport models' performance on criteria pollutants and joint analysis with meteorology, Atmospheric Chemistry and Physics, 16, 12667-12701, https://doi.org/10.5194/acp-16-12667-2016, 2016.

Carmichael, G. R., Calori, G., Hayami, H., Uno, I., Cho, S. Y., Engardt, M., Kim, S. B., Ichikawa, Y., Ikeda, Y., Woo, J. H., Ueda, H., and Amann, M.: The MICS-Asia study: model intercomparison of long-range transport and sulfur deposition in East Asia, Atmospheric Environment, 36, 175-199, https://doi.org/10.1016/S1352-2310(01)00448-4, 2002.

Carmichael, G. R., Sakurai, T., Streets, D., Hozumi, Y., Ueda, H., Park, S. U., Fung, C., Han, Z., Kajino, M., Engardt, M., Bennet, C., Hayami, H., Sartelet, K., Holloway, T., Wang, Z., Kannari, A., Fu, J., Matsuda, K., Thongboonchoo, N., and Amann, M.: MICS-Asia II: The model intercomparison study for Asia Phase II methodology and overview of findings, Atmospheric Environment, 42, 3468-3490, http://dx.doi.org/10.1016/j.atmosenv.2007.04.007, 2008.

Carmichael, G. R., and Ueda, H.: MICS-Asia II: The model intercomparison study for Asia phase II, Atmospheric Environment, 42, 3465-3467, http://dx.doi.org/10.1016/j.atmosenv.2007.10.003, 2008.

Chen, L., Gao, Y., Zhang, M., Fu, J. S., Zhu, J., Liao, H., Li, J., Huang, K., Ge, B., Wang, X., Lam, Y. F., Lin, C.-Y., Itahashi, S., Nagashima, T., Kajino, M., Yamaji, K., Wang, Z., and Kurokawa, J.: MICS-Asia III: multi-model comparison and evaluation of aerosol over East Asia, Atmos. Chem. Phys., 19, 11911–11937, https://doi.org/10.5194/acp-19-11911-2019, 2019.

519 Chen, Z. H., Cheng, S. Y., Li, J. B., Guo, X. R., Wang, W. H., and Chen, D. S.: Relationship between
520 atmospheric pollution processes and synoptic pressure patterns in northern China, Atmospheric
521 Environment, 42, 6078-6087, 10.1016/j.atmosenv.2008.03.043, 2008.

522 Clarke, A. D., Owens, S. R., and Zhou, J. C.: An ultrafine sea-salt flux from breaking waves: Implications
523 for cloud condensation nuclei in the remote marine atmosphere, J Geophys Res-Atmos, 111,
524 https://doi.org/10.1029/2005JD006565,2006.

525 Cohen, A. J., Brauer, M., Burnett, R., Anderson, H. R., Frostad, J., Estep, K., Balakrishnan, K.,
526 Brunekreef, B., Dandona, L., Dandona, R., Feigin, V., Freedman, G., Hubbell, B., Jobling, A., Kan, H.,
527 Knibbs, L., Liu, Y., Martin, R., Morawska, L., Pope, C. A., Shin, H., Straif, K., Shaddick, G., Thomas,
528 M., van Dingenen, R., van Donkelaar, A., Vos, T., Murray, C. J. L., and Forouzanfar, M. H.: Estimates
529 and 25-year trends of the global burden of disease attributable to ambient air pollution: an analysis of data
530 from the Global Burden of Diseases Study 2015, Lancet, 389, 1907-1918, 10.1016/s0140-
531 6736(17)30505-6, 2017.

532 Deng, J. J., Wang, T. J., Jiang, Z. Q., Xie, M., Zhang, R. J., Huang, X. X., and Zhu, J. L.: Characterization
533 of visibility and its affecting factors over Nanjing, China, Atmospheric Research, 101, 681-691,
534 10.1016/j.atmosres.2011.04.016, 2011.

535 Dennis, R., Fox, T., Fuentes, M., Gilliland, A., Hanna, S., Hogrefe, C., Irwin, J., Rao, S. T., Scheffe, R.,
536 Schere, K., Steyn, D., and Venkatram, A.: A framework for evaluating regional-scale numerical
537 photochemical modeling systems, Environ Fluid Mech, 10, 471-489, doi: 10.1007/s10652-009-9163-2,
538 2010.

539 Dong, X. Y., Fu, J. S., Zhu, Q. Z., Sun, J., Tan, J. N., Keating, T., Sekiya, T., Sudo, K., Emmons, L.,
540 Tilmes, S., Jonson, J. E., Schulz, M., Bian, H. S., Chin, M., Davila, Y., Henze, D., Takemura, T.,
541 Benedictow, A. M. K., and Huang, K.: Long-range transport impacts on surface aerosol concentrations
542 and the contributions to haze events in China: an HTAP2 multi-model study, Atmospheric Chemistry and
543 Physics, 18, 15581-15600, https://doi.org/10.5194/acp-18-15581-2018, 2018.

544 Fountoukis, C., and Nenes, A.: ISORROPIA II: a computationally efficient thermodynamic equilibrium
545 model for K+-Ca2+-Mg2+-Nh(4)(+)-Na+-SO42--NO3--Cl--H2O aerosols, Atmospheric Chemistry and
546 Physics, 7, 4639-4659, https://doi.org/10.5194/acp-7-4639-2007, 2007.

547 Fu, J. S., Jang, C. J., Streets, D. G., Li, Z., Kwok, R., Park, R., and Han, Z.: MICS-Asia II: Modeling
548 gaseous pollutants and evaluating an advanced modeling system over East Asia, Atmospheric
549 Environment, 42, 3571-3583, http://dx.doi.org/10.1016/j.atmosenv.2007.07.058, 2008.

550 Fuzzi, S., Baltensperger, U., Carslaw, K., Decesari, S., van Der Gon, H. D., Facchini, M. C., Fowler, D.,
551 Koren, I., Langford, B., Lohmann, U., Nemitz, E., Pandis, S., Riipinen, I., Rudich, Y., Schaap, M.,
552 Slowik, J. G., Spracklen, D. V., Vignati, E., Wild, M., Williams, M., and Gilardoni, S.: Particulate matter,
553 air quality and climate: lessons learned and future needs, Atmospheric Chemistry and Physics, 15, 8217-
554 8299, https://doi.org/10.5194/acp-15-8217-2015, 2015.

555 Galmarini, S., Koffi, B., Solazzo, E., Keating, T., Hogrefe, C., Schulz, M., Benedictow, A., Griesfeller, J.
556 J., Janssens-Maenhout, G., Carmichael, G., Fu, J., and Dentener, F.: Technical note: Coordination and
557 harmonization of the multi-scale, multi-model activities HTAP2, AQMEII3, and MICS-Asia3:
558 simulations, emission inventories, boundary conditions, and model output formats, Atmos. Chem. Phys.,
559 17, 1543-1555, 10.5194/acp-17-1543-2017, 2017.

Gong, S. L.: A parameterization of sea-salt aerosol source function for sub- and super-micron particles, Global Biogeochem Cy, 17, https://doi.org/10.1029/2003GB002079, 2003.

Han, Z., Sakurai, T., Ueda, H., Carmichael, G. R., Streets, D., Hayami, H., Wang, Z., Holloway, T., Engardt, M., Hozumi, Y., Park, S. U., Kajino, M., Sartelet, K., Fung, C., Bennet, C., Thongboonchoo, N., Tang, Y., Chang, A., Matsuda, K., and Amann, M.: MICS-Asia II: Model intercomparison and evaluation of ozone and relevant species, Atmospheric Environment, 42, 3491-3509, http://dx.doi.org/10.1016/j.atmosenv.2007.07.031, 2008.

Hayami, H., Sakurai, T., Han, Z., Ueda, H., Carmichael, G. R., Streets, D., Holloway, T., Wang, Z., Thongboonchoo, N., Engardt, M., Bennet, C., Fung, C., Chang, A., Park, S. U., Kajino, M., Sartelet, K., Matsuda, K., and Amann, M.: MICS-Asia II: Model intercomparison and evaluation of particulate sulfate, nitrate and ammonium, Atmospheric Environment, 42, 3510-3527, http://dx.doi.org/10.1016/j.atmosenv.2007.08.057, 2008.

Hoek, G., and Raaschou-Nielsen, O.: Impact of fine particles in ambient air on lung cancer, Chinese Journal of Cancer, 33, 197-203, 10.5732/cjc.014.10039, 2014.

Im, U.: Impact of sea-salt emissions on the model performance and aerosol chemical composition and deposition in the East Mediterranean coastal regions, Atmospheric Environment, 75, 329-340, https://doi.org/10.1016/j.atmosenv.2013.04.034, 2013.

Itahashi, S., Ge, B., Sato, K., Fu, J. S., Wang, X., Yamaji, K., Nagashima, T., Li, J., Kajino, M., Liao, H., Zhang, M., Wang, Z., Li, M., Kurokawa, J., Carmichael, G. R., and Wang, Z.: MICS-Asia III: Overview of model inter-comparison and evaluation of acid deposition over Asia, Atmos. Chem. Phys. Discuss., https://doi.org/10.5194/acp-2019-624, accepted, 2019

Kelly, J. T., Bhave, P. V., Nolte, C. G., Shankar, U., and Foley, K. M.: Simulating emission and chemical evolution of coarse sea-salt particles in the Community Multiscale Air Quality (CMAQ) model, Geoscientific Model Development, 3, 257-273, https://doi.org/10.5194/gmd-3-257-2010, 2010.

Knol, A. B., de Hartog, J. J., Boogaard, H., Slottje, P., van der Sluijs, J. P., Lebret, E., Cassee, F. R., Wardekker, A., Ayres, J. G., Borm, P. J., Brunekreef, B., Donaldson, K., Forastiere, F., Holgate, S. T., Kreyling, W. G., Nemery, B., Pekkanen, J., Stone, V., Wichmann, H. E., and Hoek, G.: Expert elicitation on ultrafine particles: likelihood of health effects and causal pathways, Particle and Fibre Toxicology, 6, 10.1186/1743-8977-6-19, 2009.

Lamarque, J. F., Shindell, D. T., Josse, B., Young, P. J., Cionni, I., Eyring, V., Bergmann, D., Cameron-Smith, P., Collins, W. J., Doherty, R., Dalsoren, S., Faluvegi, G., Folberth, G., Ghan, S. J., Horowitz, L. W., Lee, Y. H., MacKenzie, I. A., Nagashima, T., Naik, V., Plummer, D., Righi, M., Rumbold, S. T., Schulz, M., Skeie, R. B., Stevenson, D. S., Strode, S., Sudo, K., Szopa, S., Voulgarakis, A., and Zeng, G.: The Atmospheric Chemistry and Climate Model Intercomparison Project (ACCMIP): overview and description of models, simulations and climate diagnostics, Geoscientific Model Development, 6, 179-206, 10.5194/gmd-6-179-2013, 2013.

Lelieveld, J., Evans, J. S., Fnais, M., Giannadaki, D., and Pozzer, A.: The contribution of outdoor air pollution sources to premature mortality on a global scale, Nature, 525, 367-+, 10.1038/nature15371, 2015.

599 Li, J., Wang, Z. F., Zhuang, G., Luo, G., Sun, Y., and Wang, Q.: Mixing of Asian mineral dust with
600 anthropogenic pollutants over East Asia: a model case study of a super-duststorm in March 2010,
601 Atmospheric Chemistry and Physics, 12, 7591-7607, DOI: 10.5194/acp-12-7591-2012, 2012.

602 Li, M., Zhang, Q., Kurokawa, J. I., Woo, J. H., He, K., Lu, Z., Ohara, T., Song, Y., Streets, D. G.,
603 Carmichael, G. R., Cheng, Y., Hong, C., Huo, H., Jiang, X., Kang, S., Liu, F., Su, H., and Zheng, B.:
604 MIX: a mosaic Asian anthropogenic emission inventory under the international collaboration framework
605 of the MICS-Asia and HTAP, Atmos. Chem. Phys., 17, 935-963, 10.5194/acp-17-935-2017, 2017.

606 Li, J., Chen, X. S., Wang, Z. F., Du, H. Y., Yang, W. Y., Sun. Y. L., Hu, B., Li, J. J., Wang. W., Wang.
607 T., Fu, P. Q., Huang, H. L.: Radiative and heterogeneous chemical effects of aerosols on ozone and
608 inorganic aerosols over East Asia, Sci. Total Environ. 622-623, 1327-1342,
609 10.1016/j.scitotenv.2017.12.041.

610 Liao, H., Adams, P. J., Chung, S. H., Seinfeld, J. H., Mickley, L. J., and Jacob, D. J.: Interactions between
611 tropospheric chemistry and aerosols in a unified general circulation model, J. Geophys. Res., 108 (D1),
612 4001, doi:10.1029/2001JD001260, 2003.

613 Lippmann, M.: Toxicological and epidemiological studies of cardiovascular effects of ambient air fine
614 particulate matter (PM2.5) and its chemical components: Coherence and public health implications, Crit
615 Rev Toxicol, 44, 299-347, DOI: 10.3109/10408444.2013.861796, 2014.

616 Liu, Y. M., Zhang, S. T., Fan, Q., Wu, D., Chan, P. W., Wang, X. M., Fan, S. J., Feng, Y. R., and Hong,
617 Y. Y.: Accessing the Impact of Sea-Salt Emissions on Aerosol Chemical Formation and Deposition over
618 Pearl River Delta, China, Aerosol Air Qual Res, 15, 2232-2245, doi: 10.4209/aaqr.2015.02.0127, 2015.

619 Nel, A.: Air pollution-related illness: Effects of particles, Science, 308, 804-806, DOI:
620 10.1126/science.1108752, 2005.

621 Qu, W. J., Arimoto, R., Zhang, X. Y., Zhao, C. H., Wang, Y. Q., Sheng, L. F., and Fu, G.: Spatial
622 distribution and interannual variation of surface PM10 concentrations over eighty-six Chinese cities,
623 Atmospheric Chemistry and Physics, 10, 5641-5662, 10.5194/acp-10-5641-2010, 2010.

624 Rao, S., Chirkov, V., Dentener, F., Van Dingenen, R., Pachauri, S., Purohit, P., Amann, M., Heyes, C.,
625 Kinney, P., Kolp, P., Klimont, Z., Riahi, K., and Schoepp, W.: Environmental Modeling and Methods for
626 Estimation of the Global Health Impacts of Air Pollution, Environmental Modeling & Assessment, 17,
627 613-622, 10.1007/s10666-012-9317-3, 2012.

628 Shao, Y., Dong, C. H. A review on East Asian dust storm climate, modeling and moni-toring: Global and
629 Planetary Change, 2006, 52(1-4): 1-22.

630 Silva, R. A., West, J. J., Zhang, Y. Q., Anenberg, S. C., Lamarque, J. F., Shindell, D. T., Collins, W. J.,
631 Dalsoren, S., Faluvegi, G., Folberth, G., Horowitz, L. W., Nagashima, T., Naik, V., Rumbold, S., Skeie,
632 R., Sudo, K., Takemura, T., Bergmann, D., Cameron-Smith, P., Cionni, I., Doherty, R. M., Eyring, V.,
633 Josse, B., MacKenzie, I. A., Plummer, D., Righi, M., Stevenson, D. S., Strode, S., Szopa, S., and Zeng,
634 G.: Global premature mortality due to anthropogenic outdoor air pollution and the contribution of past
635 climate change, Environ Res Lett, 8, 10.1088/1748-9326/8/3/034005, 2013.

636 Tebaldi, C., and Knutti, R.: The use of the multi-model ensemble in probabilistic climate projections,
637 Philos T R Soc A, 365, 2053-2075, https://doi.org/10.1098/rsta.2007.2076, 2007.

638 Tie, X., Madronich, S., Walters, S., Edwards, D. P., Ginoux, P., Mahowald, N., Zhang, R., Lou, C.,
639 and Brasseur, G.: Assessment of the global impact of aerosols on tropospheric oxidants, J. Geophys.
640 Res., 110, D03204, doi:10.1029/2004JD005359, 2005.

641 Vivanco, M. G., Bessagnet, B., Cuvelier, C., Theobald, M. R., Tsyro, S., Pirovano, G., Aulinger, A.,
642 Bieser, J., Calori, G., Ciarelli, G., Manders, A., Mircea, M., Aksoyoglu, S., Briganti, G., Cappelletti, A.,
643 Colette, A., Couvidat, F., D'Insidoro, M., Kranenburg, R., Meleux, F., Menut, L., Pay, M. T., Rouil, L.,
644 Silibello, C., Thunis, P., and Ung, A.: Joint analysis of deposition fluxes and atmospheric concentrations
645 of inorganic nitrogen and sulphur compounds predicted by six chemistry transport models in the frame of
646 the EURODELTAIII project, Atmospheric Environment, 151, 152-175,
647 https://doi.org/10.1016/j.atmosenv.2016.11.042, 2017.

648 Wang, K., Zhang, Y., Nenes, A., and Fountoukis, C.: Implementation of dust emission and chemistry into
649 the Community Multiscale Air Quality modeling system and initial application to an Asian dust storm
650 episode, Atmospheric Chemistry and Physics, 12, 10209-10237, https://doi.org/10.5194/acp-12-10209-
651 2012, 2012.

652 Wesely, M. L.: Parameterization of Surface Resistances to Gaseous Dry Deposition in Regional-Scale
653 Numerical-Models, Atmospheric Environment, 23, 1293-1304, https://doi.org/10.1016/0004-
654 6981(89)90153-4, 1989.

655 Xing, J., Mathur, R., Pleim, J., Hogrefe, C., Gan, C. M., Wong, D. C., Wei, C., Gilliam, R., and Pouliot,
656 G.: Observations and modeling of air quality trends over 1990-2010 across the Northern Hemisphere:
657 China, the United States and Europe, Atmospheric Chemistry and Physics, 15, 2723-2747, 10.5194/acp-
658 15-2723-2015, 2015.

659 Zhang, L., Brook, J. R., and Vet, R.: A revised parameterization for gaseous dry deposition in air-quality
660 models, Atmospheric Chemistry and Physics, 3, 2067-2082, https://doi.org/10.5194/acp-3-2067-2003,
661 2003.

662

663

Figures and tables

Figure 1

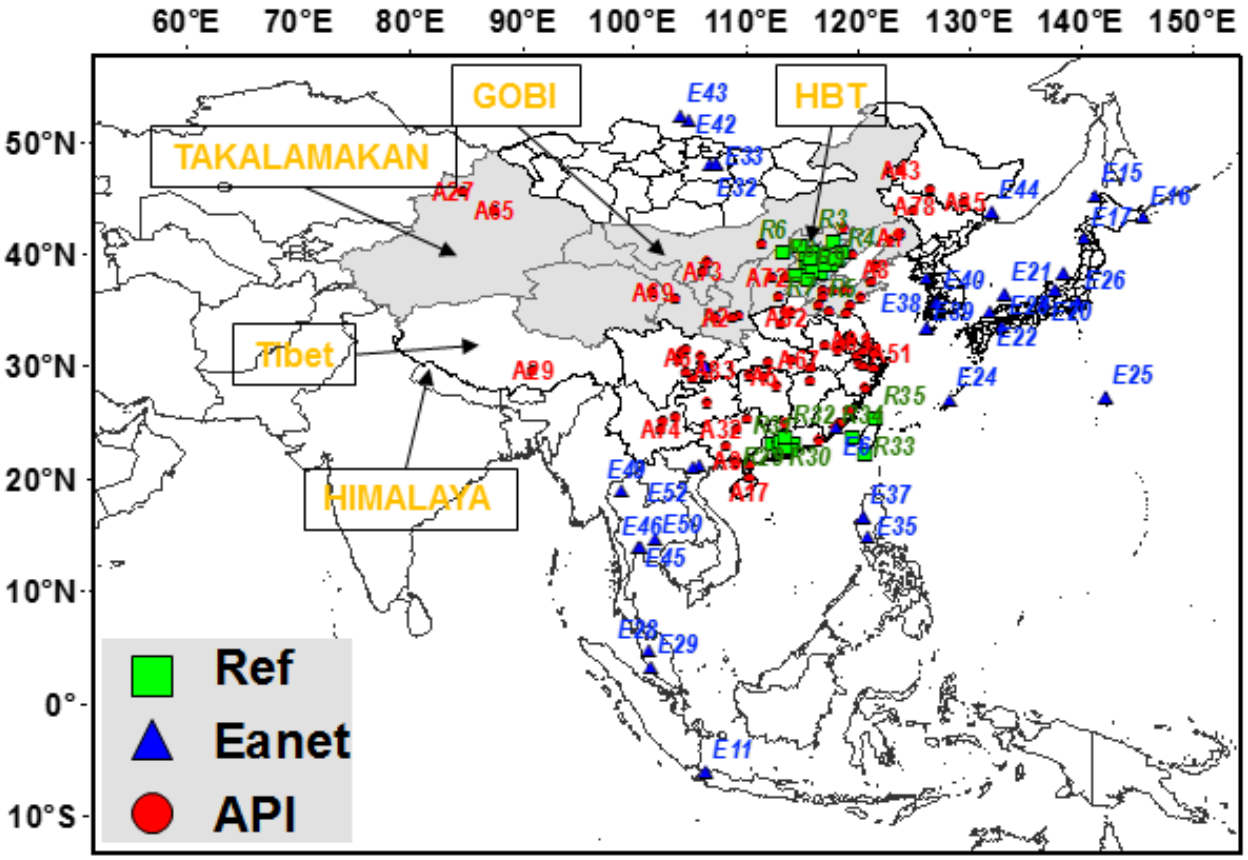

Figure 1 The geographical locations of observation networks of API (red color, A1-A86), EANET (blue color, E1-E54, only sites with available observation during simulation time are shown) and Ref (green color, R1-R35) sites. Grey shaded regions have been reported to be affected by dust storms.

671 **Figure 2**

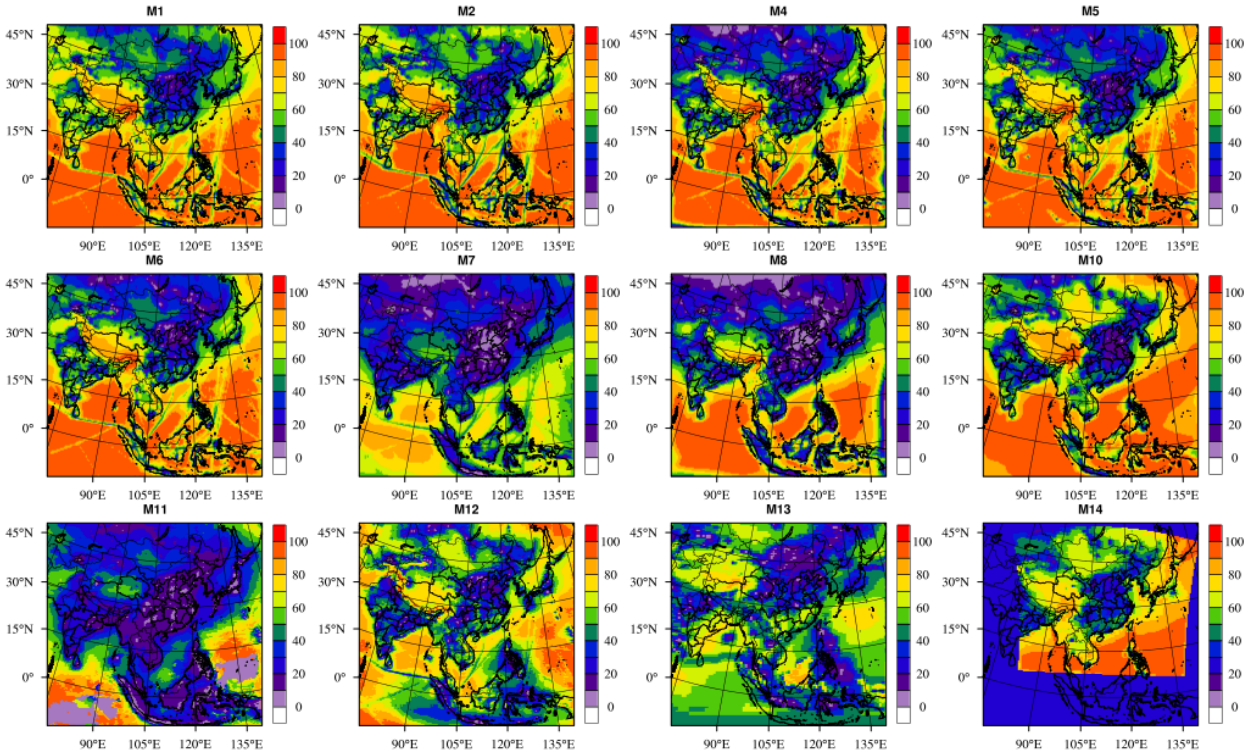

672
673 Figure 2 *SOR* values at surface layer for models (unit: %). *SOR* is calculated by $SO_4^{2-}/(SO_2+SO_4^{2-})\times100\%$. The SO_2
674 and SO_4^{2-} concentrations are transferred from ppb and μg m^{-3} to mole(S) m^{-3} before calculating *SOR*. Values are
675 calculated by annual average data.
676

677 **Figure 3**

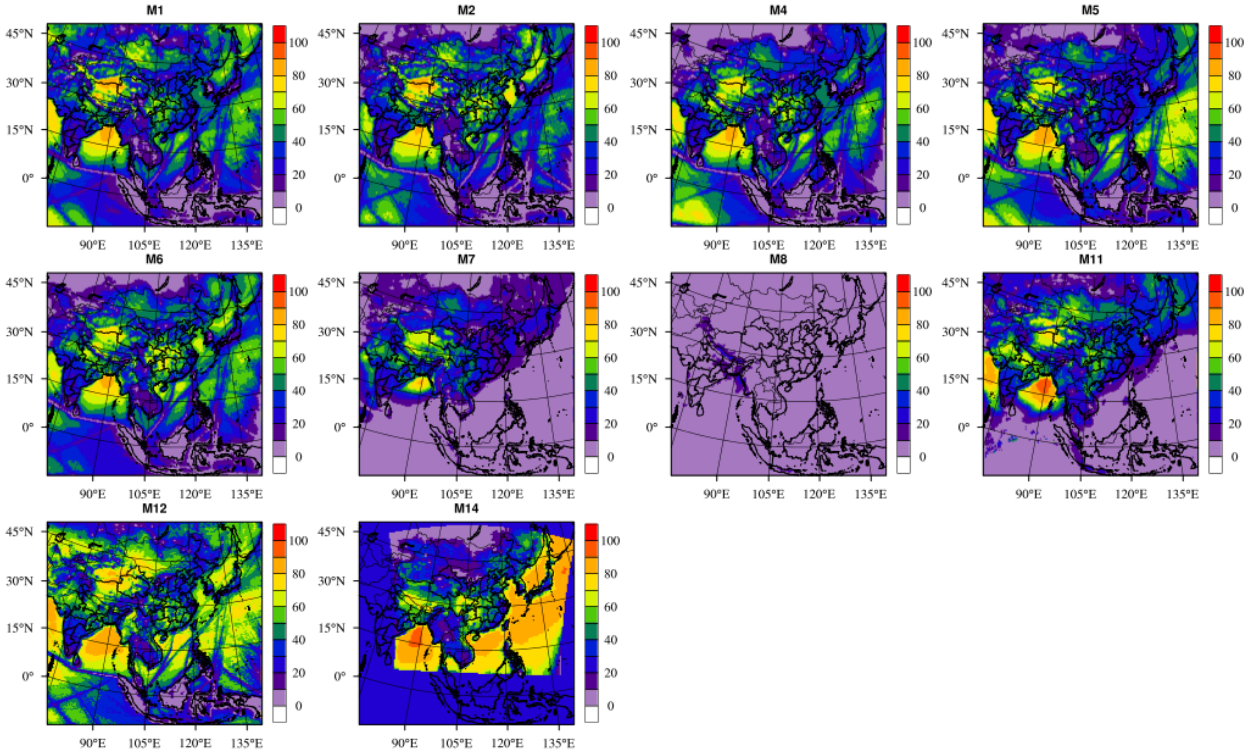

678
679 Figure 3 Same as Fig.2 but for *C(NO₂)* (unit: %). *C(NO₂)* is calculated by $NO_3^-/(NO_2+NO_3^-)\times100\%$. The *C(NO₂)* of
680 M8 is extremely low due to unreasonable low NO_3^- concentration, which is considered as outliner in this study. Values
681 are calculated by annual average data.

682 **Figure 4**

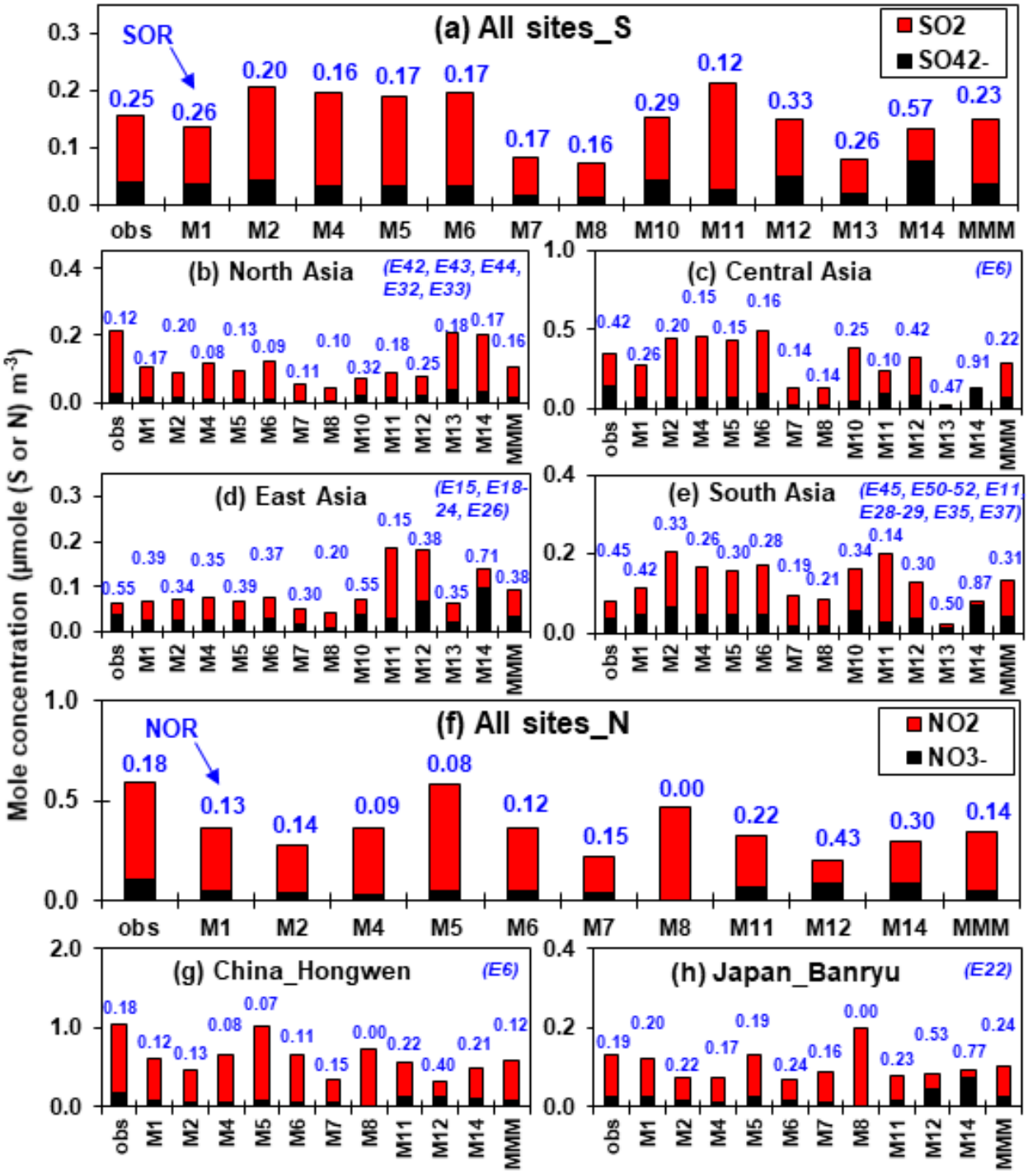

683
684 Figure 4 Gas-particle conversions of S and N of observation and models at EANET sites. The unit is µmole (S or N)
685 m^{-3}. The red bars and black bars represent the concentrations of gases and aerosols. The blue-color values above the
686 bars are observed/modelled *SOR* and *C(NO_2)*. Values are calculated with annual average concentrations. The
687 concentrations of gases and aerosols are all transferred to µmole (S or N) m^{-3} before calculation. The blue-color
688 numbers on top-right (e.g. E22) are site numbers. The locations of the sites are illustrated in Fig. 1. Results for
689 individual sites are shown in supplementary Fig. S1.

690 **Figure 5**

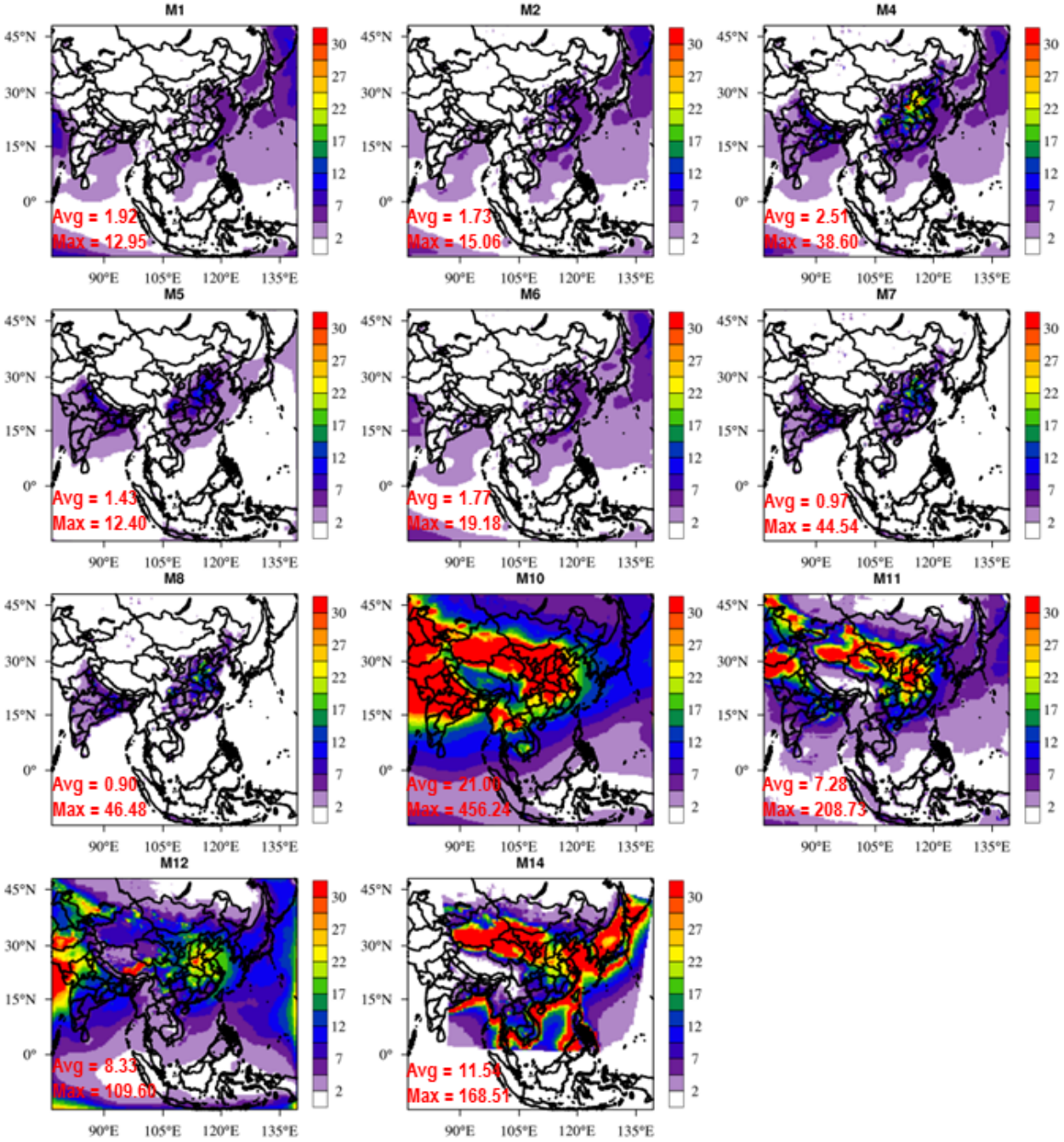

691
692 Figure 5 Annual average PMC concentrations at surface layer of individual models (μg m^{-3}). The value is calculated
693 by subtracting $PM_{2.5}$ from PM_{10}. The values in left-bottom are domain average (Avg) and maximum (Max) values.
694

Figure 6

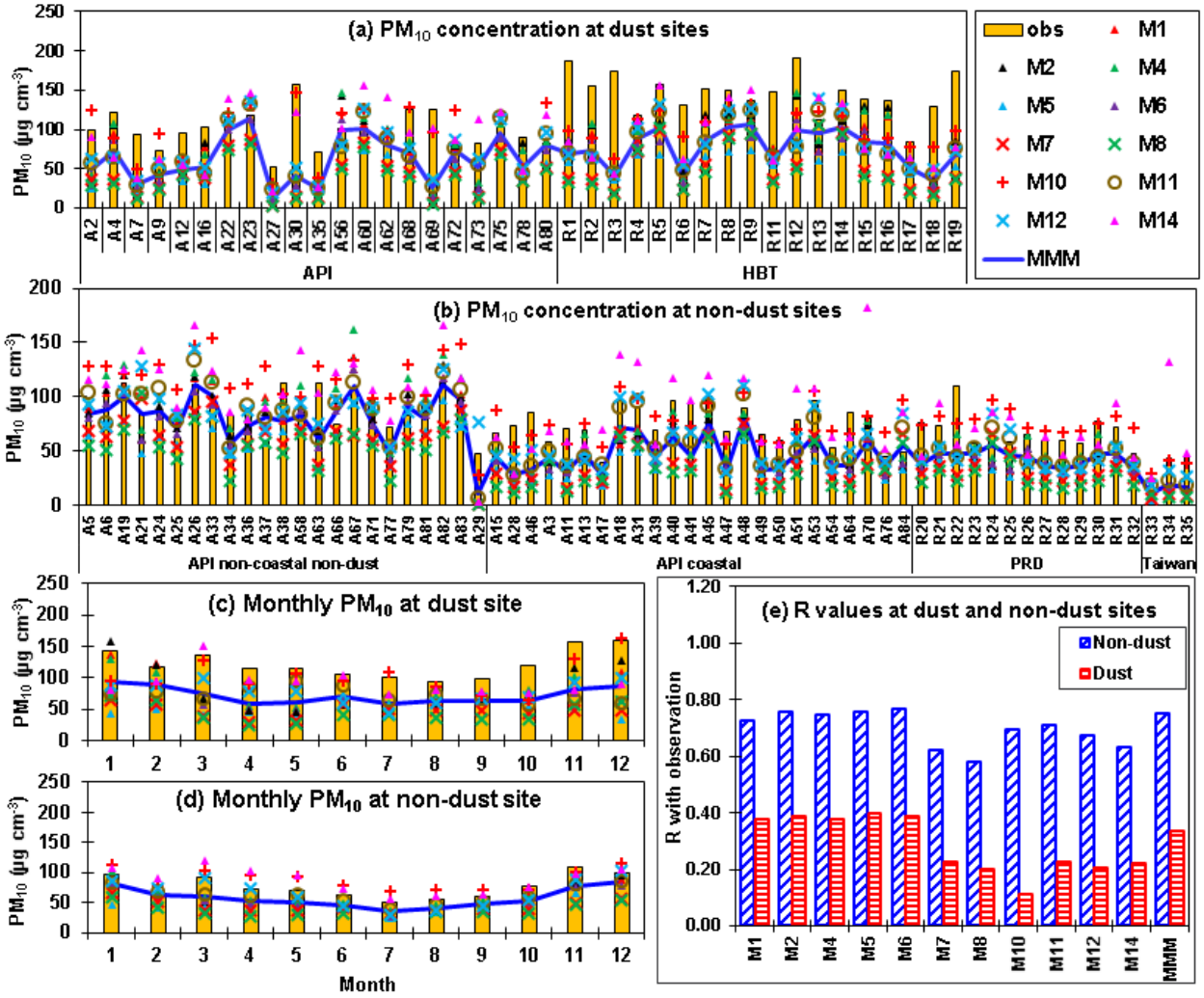

Figure 6 Multi-model performances on (a-b) annual average PM_{10} concentrations at the dust sites and non-dust sites and (c-d) monthly average PM_{10} concentrations at the dust sites and non-dust sites. X axis for (a-b) indicates site numbers. The locations of the sites are illustrated in figure 1. The yellow bars are observations, the blue lines are the MMM and different markers represent individual model results. (e) R values of models with observations at the dust and non-dust sites.

704 **Figure 7**

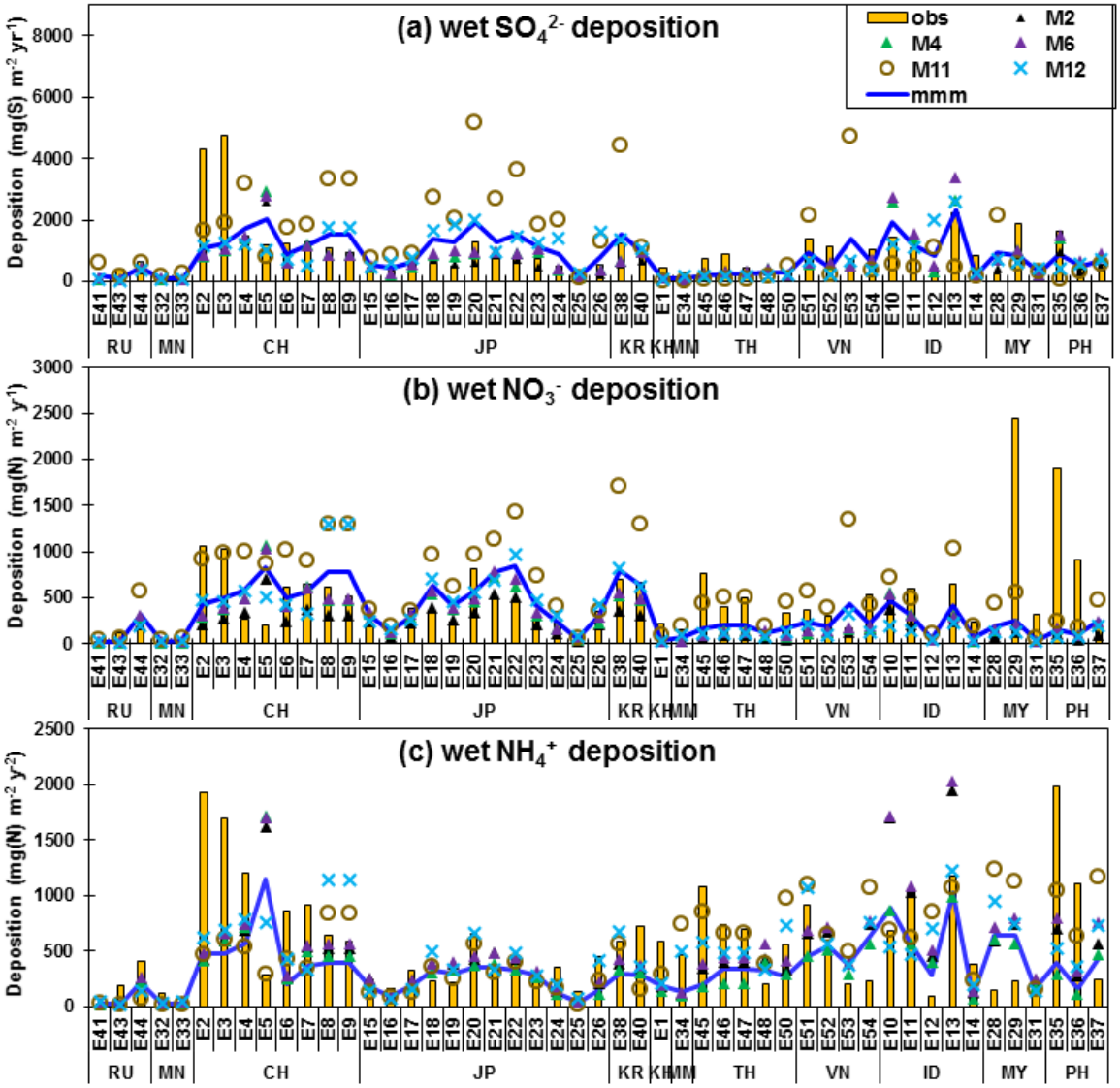

705
706 Figure 7 Modelled annual-accumulated wet deposition of SO_4^{2-}, NO_3^- and NH_4^+ compared with observation from
707 EANET network. The units are mg(S or N) m^{-2} yr^{-1}. Abbreviation for regions: RU-Russia, MN-Mongolia, CH-
708 China, JP-Japan, KR-Korea, KH-Cambodia, MN-Myanmar, TH-Thailand, VN-Vietnam, ID-Indonesia, MY-
709 Malaysia, PH-Philippine.
710

711 **Figure 8**

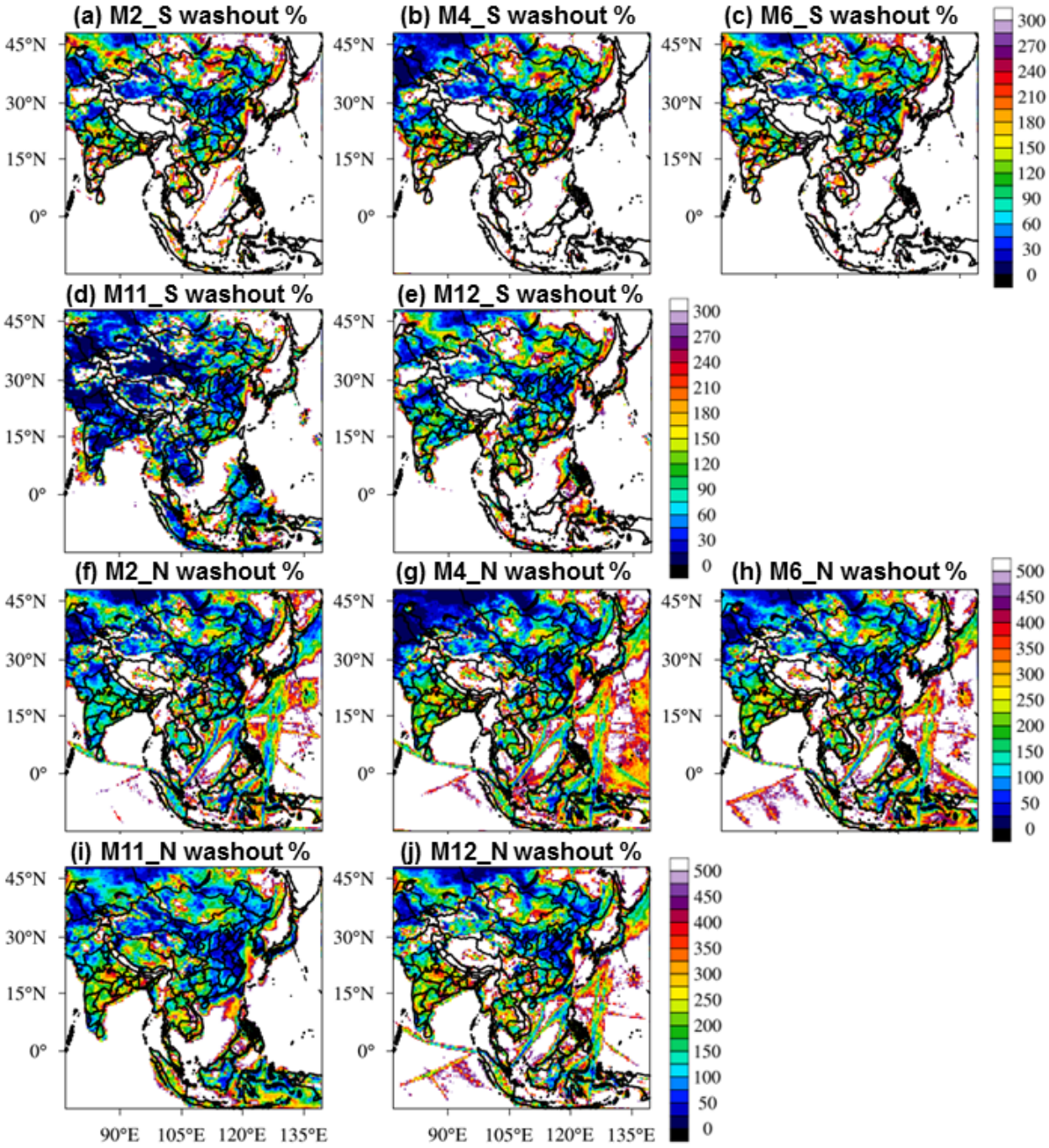

712
713 Figure 8 Washout ratios (λ_{wet}) of (a-e) S deposition and (f-j) N deposition of models. Values are calculated with
714 annual accumulated depositions. The unit is %.
715

716 **Figure 9**

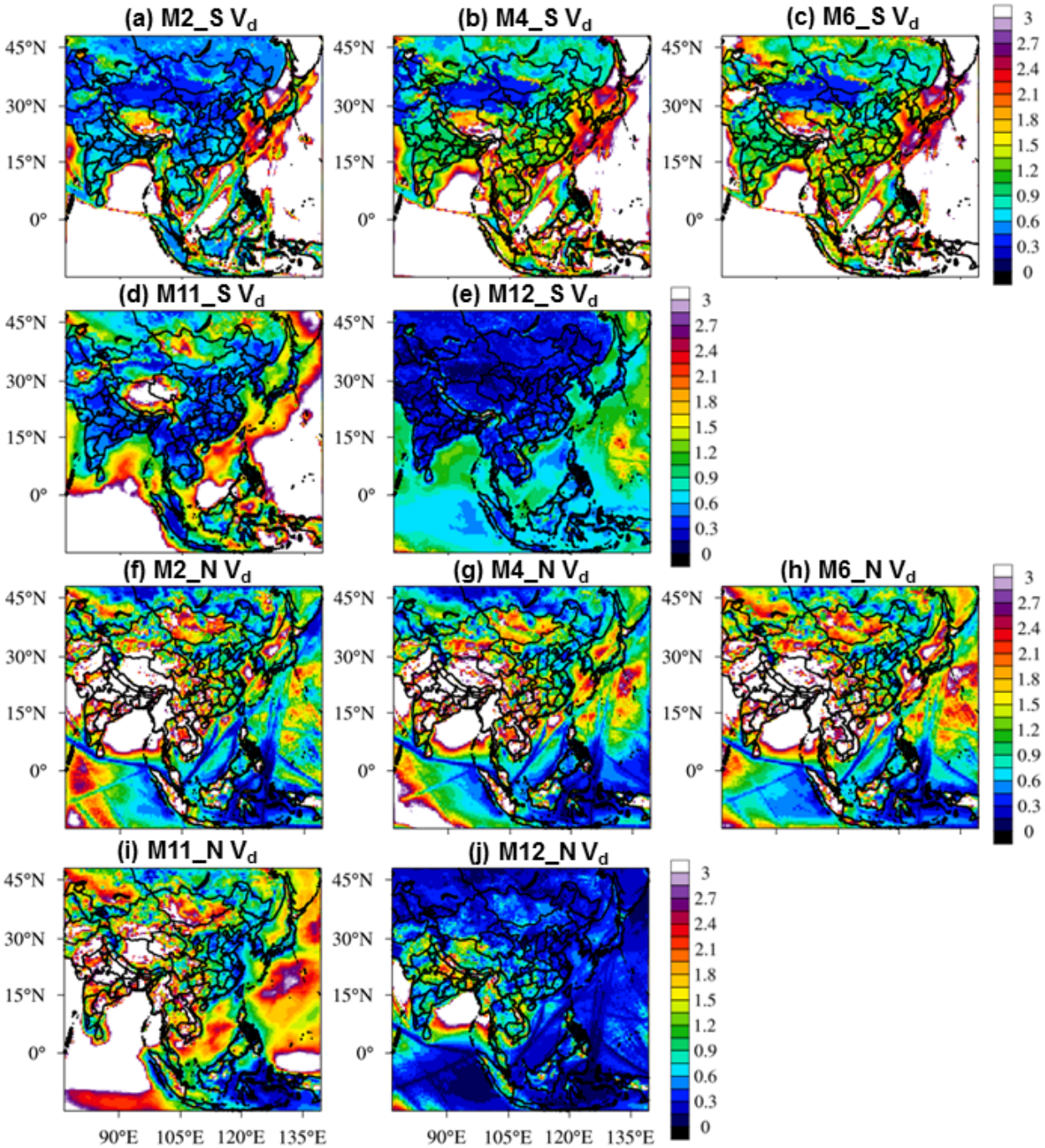

717
718 Figure 9 Dry deposition velocities (V_d) of (a-e) S deposition and (f-j) N deposition of models. Values are calculated
719 with annual accumulated depositions. The unit is cm s^{-1}.
720

Table 1

Table 1 Multi-model performance on annual average concentrations of PM_{10} at the dust and non-dust sites (unit: $\mu g\ m^{-3}$)

Dust site	M1	M2	M4	M5	M6	M7	M8	M10	M11	M12	M14	MMM
Mean Obs						120.7						
Mean MMM	77.2	82.2	81.6	51.7	65.6	47.5	44.3	102.5	73.5	77.3	92.1	69.2
S	0.4	0.4	0.4	0.3	0.3	0.2	0.2	0.1	0.2	0.2	0.3	0.3
MB	-43.5	-38.5	-39.2	-69.0	-55.1	-73.2	-76.4	-18.2	-47.2	-43.4	-28.6	-51.5
R	0.4	0.4	0.4	0.4	0.4	0.2	0.2	0.1	0.2	0.2	0.2	0.3
F	66.7	69.2	69.2	38.5	56.4	35.9	33.3	84.6	59.0	66.7	66.7	66.7
NMB (%)	-36.1	-31.9	-32.4	-57.2	-45.7	-60.6	-63.3	-15.1	-39.1	-36.0	-23.7	-42.6
NME (%)	38.3	35.4	36.4	57.2	46.2	60.6	63.3	32.8	42.3	40.5	36.1	42.7
MFB (%)	-49.4	-44.6	-44.6	-83.4	-64.1	-92.9	-98.8	-19.3	-51.8	-46.8	-31.7	-56.9
MFE (%)	51.8	48.3	48.7	83.4	64.7	92.9	98.8	36.1	55.3	51.7	44.5	56.9
Number of Sites						39						

Table 1 Continued

Non-dust site	M1	M2	M4	M5	M6	M7	M8	M10	M11	M12	M14	MMM
Mean Obs						77.2						
Mean MMM	58.2	58.5	66.5	45.2	55.2	44.8	39.0	90.0	64.4	66.3	89.5	57.8
S	1.0	1.1	1.2	0.8	1.0	0.7	0.6	1.0	1.0	0.9	1.1	0.9
MB	-19.0	-18.7	-10.8	-32.1	-22.1	-32.5	-38.3	12.7	-12.9	-10.9	12.2	-19.4
R	0.7	0.8	0.7	0.8	0.8	0.6	0.6	0.7	0.7	0.7	0.6	0.8
F	82.5	81.0	84.1	66.7	82.5	52.4	46.0	85.7	90.5	93.7	84.1	82.5
NMB (%)	-24.6	-24.2	-14.0	-41.5	-28.6	-42.0	-49.5	16.5	-16.6	-14.1	15.8	-25.1
NME (%)	30.7	30.7	27.3	41.5	31.4	43.9	50.7	25.7	26.3	26.1	30.8	28.0
MFB (%)	-36.8	-37.5	-25.1	-59.2	-41.8	-62.0	-75.0	13.1	-24.9	-20.3	8.3	-34.6
MFE (%)	42.0	42.8	35.3	59.2	44.4	64.0	76.1	23.4	33.5	31.3	29.1	37.5
Number of Sites						63						

728 **Table 2**

729 Table 2 Multi-model performances on wet deposition (unit: mg(S or N) m^{-2} y^{-1})

	Wet SO_4^{2-} Deposition						Wet NO_3^- Deposition					
	M2	M4	M6	M11	M12	MMM	M2	M4	M6	M11	M12	MMM
Mean Obs	931.3	931.3	931.3	931.3	931.3	931.3	460.9	460.9	460.9	460.9	460.9	460.9
Mean MMM	633.7	724.2	775	1313.2	826.2	854.5	187.5	266.7	279.5	597.8	308.3	328
S	0.3	0.3	0.3	0.3	0.2	0.3	0.1	0.1	0.1	0.2	0.1	0.1
MB	-297.7	-207.1	-156.3	381.9	-105.1	-76.9	-273.4	-194.2	-181.4	137	-152.6	-132.9
R	0.5	0.4	0.4	0.2	0.3	0.4	0.1	0.2	0.2	0.2	0.1	0.2
F	61.2	61.2	61.2	24.5	40.8	51	38.8	49	46.9	44.9	38.8	46.9
NMB	-32	-22.2	-16.8	41	-11.3	-8.3	-59.3	-42.1	-39.4	29.7	-33.1	-28.8
NME	49.3	50.2	51.5	117.3	62.8	53.6	66.2	60.9	60.6	78.4	68.8	58.2
MFB	-37.4	-23.4	-15.8	4.6	-11.4	-4.6	-75.8	-49.8	-42.1	25.8	-40.9	-27.6
MFE	57.8	55.9	53.7	93.8	66.7	57.6	84.9	71.2	69.3	61	74.6	62.3
Number of Sites	49	49	49	49	49	49	49	49	49	49	49	49

730

731 Table 2 Continued

	Wet NH_4^+ Deposition					
	M2	M4	M6	M11	M12	MMM
Mean Obs	558.4	558.4	558.4	558.4	558.4	558.4
Mean MMM	459.9	349.4	497.4	505	478	337.6
S	0.3	0.1	0.3	0.3	0.2	0.2
MB	-98.5	-208.9	-61	-53.4	-80.4	-220.7
R	0.3	0.2	0.3	0.4	0.4	0.3
F	40.8	44.9	44.9	51	46.9	38.8
NMB	-17.6	-37.4	-10.9	-9.6	-14.4	-39.5
NME	64.8	65.5	64.9	58.2	57	63.6
MFB	-21.2	-42.4	-14.4	-18	-12.6	-41.9
MFE	70.7	77.9	69.1	65.9	62.9	76.1
Number of sites	49	49	49	49	49	49

732

733

Table 3

Table 3 Domain-total annual-accumulated S and N depositions of models (Tg(S or N) yr^{-1}). Empty values mean no model submissions or the values are 0.

Model	Wet S deposition				Dry S deposition			
	SO_2	H_2SO_4	SO_4^{2-}	Total Wet S	SO_2	H_2SO_4	SO_4^{2-}	Total Dry S
M1	0.06	-	-	-	-	-	-	-
M2	0.04	-	10.4	10.5	3.4	0.01	0.9	4.3
M4	0.06	-	12.5	12.5	6.6	0.01	1.1	7.6
M5	-	-	-	-	-	-	-	-
M6	0.05	-	13.7	13.8	6.3	0.01	1.4	7.7
M7	-	-	-	-	-	-	-	-
M8	-	-	-	-	-	-	-	-
M10	-	-	-	-	-	-	-	-
M11	1.1	0.3	29.9	31.3	6.9	2.2	1.5	10.6
M12	-	-	16.3	16.3	3.7	-	0.4	4.2
M13	6.0	-	-	-	-	-	-	-
M14	0.02	-	6.2	-	5.4	-	3.2	-

Table 3 Continued

Model	Wet N deposition					Dry N deposition						
	NO_3^-	NH_4^+	HNO_3	NH_3	Total Wet N	NO	NO_2	NO_3^-	NH_4^+	HNO_3	NH_3	Total Dry N
M1	-	-	-	-	-	-	-	-	-	4.3	6.9	-
M2	4.0	8.3	-	-	12.2	0.03	0.4	0.6	0.6	2.0	7.5	11.0
M4	5.4	7.4	-	-	12.8	0.03	0.3	0.7	0.5	2.8	4.7	9.0
M5	-	-	-	-	-	-	0.5	-	-	-	-	-
M6	5.6	9.1	-	-	14.6	0.02	0.3	0.8	0.7	2.9	6.5	11.1
M7	-	-	-	-	-	-	-	-	-	-	-	-
M8	-	-	-	-	-	-	-	-	-	-	-	-
M10	-	-	-	-	-	-	-	-	-	-	-	-
M11	1.5	2.8	8.1	7.6	20.0	-	-	1.3	2.4	3.3	7.1	14.1
M12	5.4	11.0	-	-	16.5	0.04	0.4	0.4	0.3	0.5	2.2	3.9
M13	-	-	4.1	-	-	-	-	-	-	4.5	4.6	-
M14	-	-	-	-	-	-	-	-	-	-	-	-